Supporting Information

Angular-dependent Magnetoresistance Modulated by Interfacial Magnetic State in Pt/LSMO Heterostructures

Ruikang Li,[1] Chao Jin,[1*] Xingmo Zhang,[2] Jiangtao Qu,[3] Dongxing Zheng,[4] Wenxue He,[1,5] Fan Yang,[1,5] Rongkun Zheng,[2] and Haili Bai[1]

[1]*Tianjin Key Laboratory of Low Dimensional Materials Physics and Processing Technology, School of Science, Tianjin University, Tianjin 300350, China*

[2]*School of Physics, The University of Sydney, Sydney, NSW 2006, Australia*

[3]*Australian Centre for Microscopy & Microanalysis, The University of Sydney, Sydney, NSW 2006, Australia*

[4]*Physical Science and Engineering Division, King Abdullah University of Science and Technology, Thuwal 23955-6900, Saudi Arabia*

[5]*Center for Joint Quantum Studies, School of Science, Tianjin University, Tianjin 300350, China*

[*]Author to whom all correspondence should be addressed.

E-mail: chaojin@tju.edu.cn

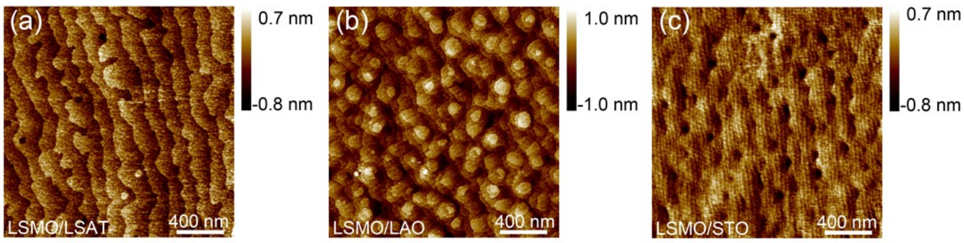

Fig. S1 Atomic force microscopy images of LSMO films on (a) LSAT, (b) LAO, and (c) STO substrates.

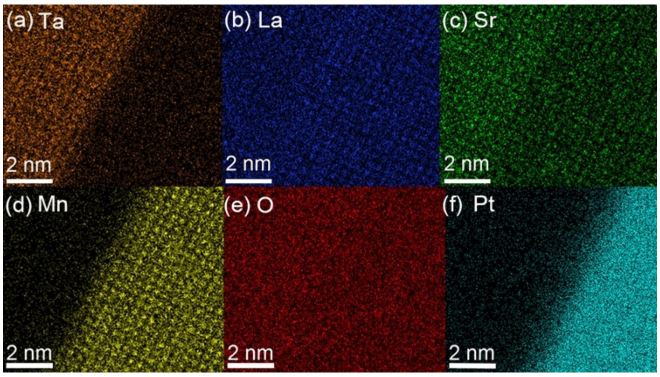

Fig. S2 Energy dispersive spectroscopy mapping of Ta, La, Sr, Mn, O, and Pt elements of LSMO/LSAT and Pt/LSMO interfaces.

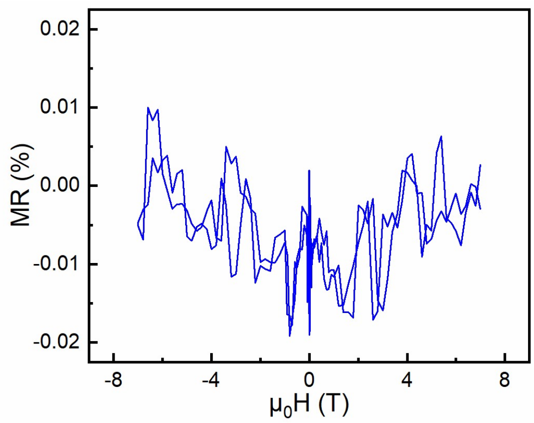

Fig. S3 FDMR curve of Pt single layer (3 nm) on STO ($H \| z$) at 100 K.

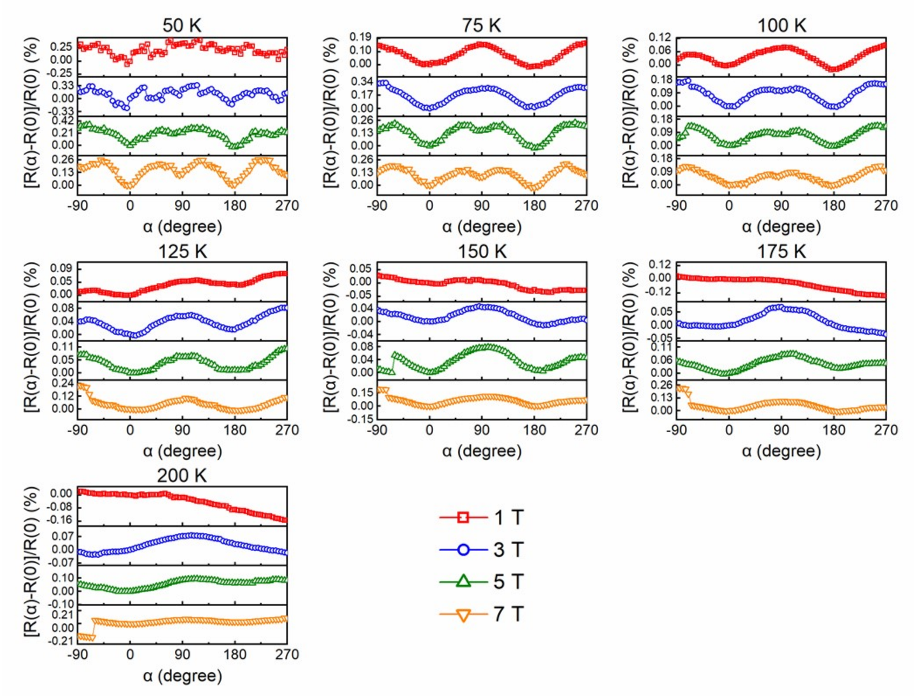

Fig. S4 ADMR curves of Pt(3 nm)/LSMO(20 nm)/LAO in the *xy* plane.

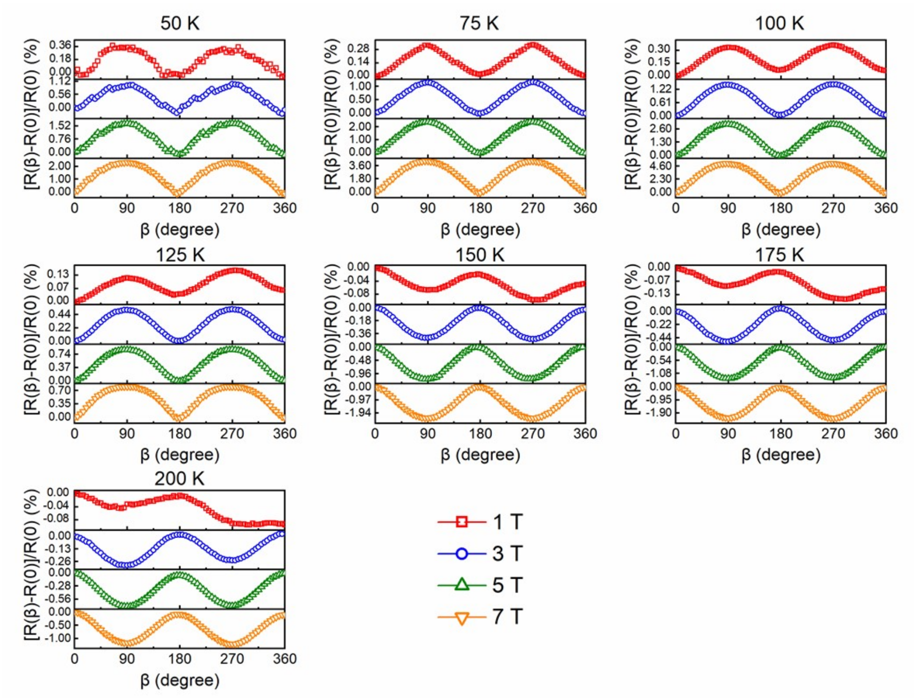

Fig. S5 ADMR curves of Pt(3 nm)/LSMO(20 nm)/LAO in the *yz* plane.

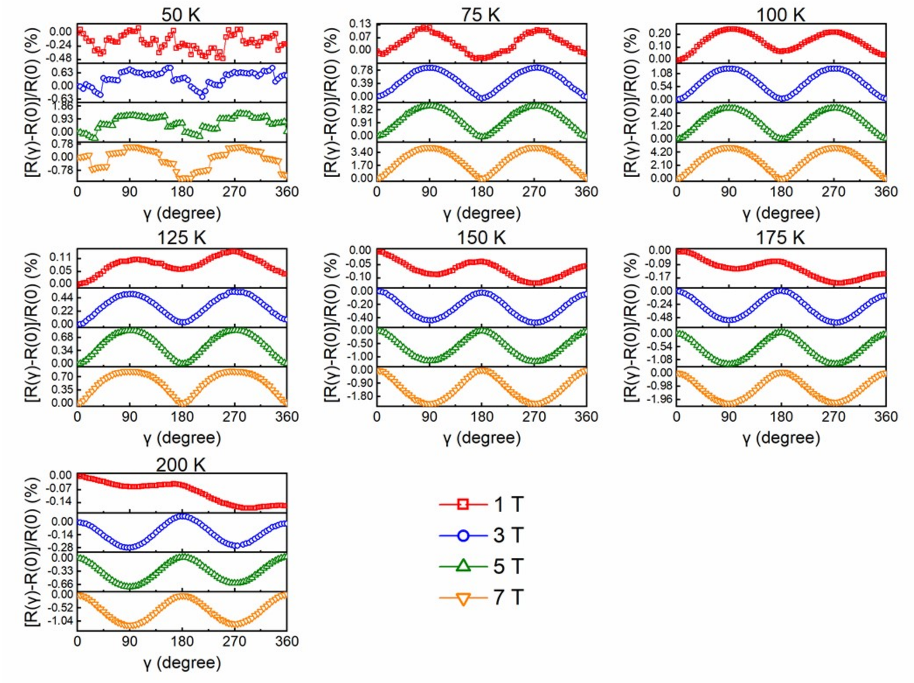

Fig. S6 ADMR curves of Pt(3 nm)/LSMO(20 nm)/LAO in the *xz* plane.

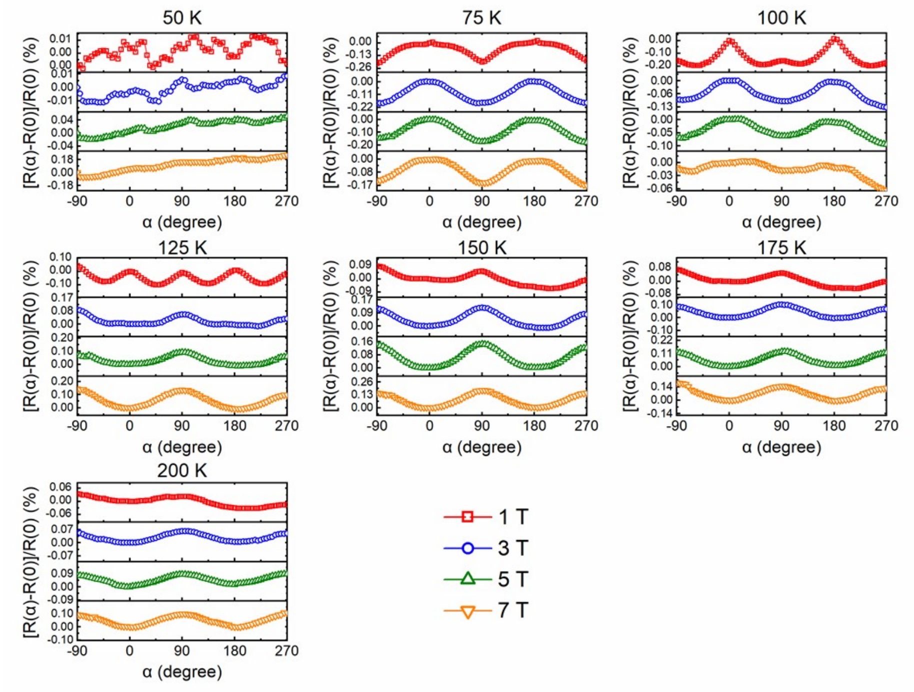

Fig. S7 ADMR curves of Pt(3 nm)/LSMO(20 nm)/STO in the *xy* plane.

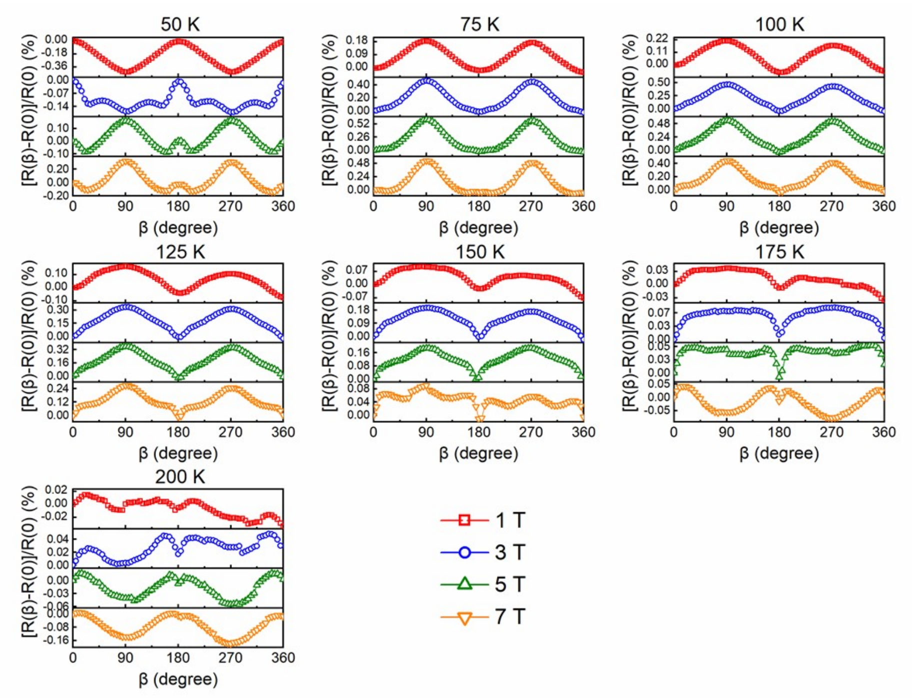

Fig. S8 ADMR curves of Pt(3 nm)/LSMO(20 nm)/STO in the *yz* plane.

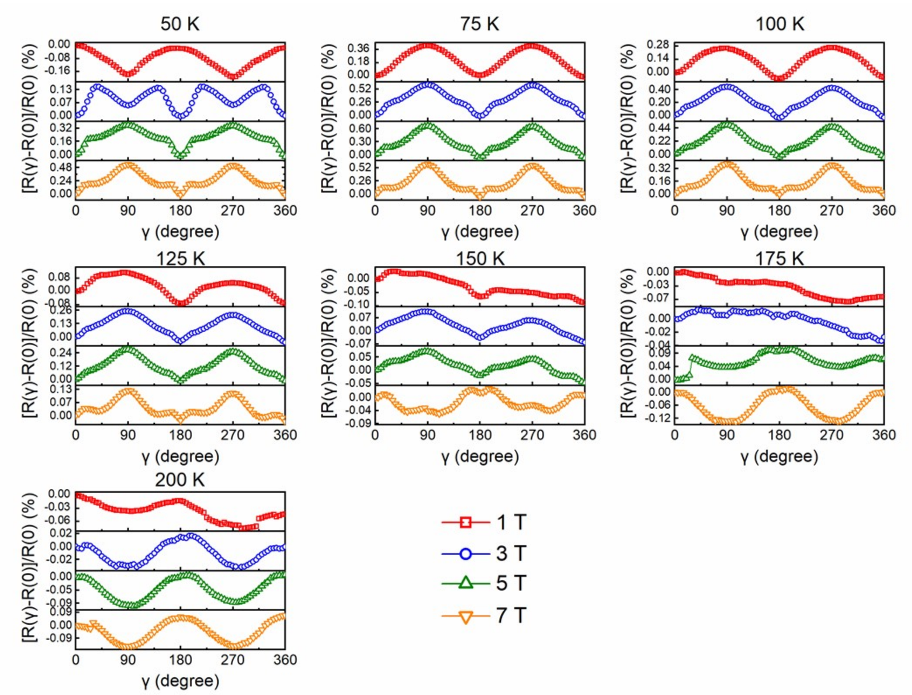

Fig. S9 ADMR curves of Pt(3 nm)/LSMO(20 nm)/STO in the *xz* plane.

Tab. S1 Transition temperatures of ρ_{xx}-T, FDMR, and ADMR curves. T_{MIT} refers to the metal-insulating transition temperature of the ρ_{xx}-T curve. T_{FDMRT} and $T_{\mathrm{ADMR}(\beta,\ \gamma)\mathrm{T}}$ are the positive and negative transition temperatures for FDMR and ADMR, respectively.

	T_{MIT} (K)	T_{FDMRT} (K)	$T_{\mathrm{ADMR}(\beta,\ \gamma)\mathrm{T}}$ (K)
LAO	140	125-150	125-150
STO	56	50-75	(50-75)/150

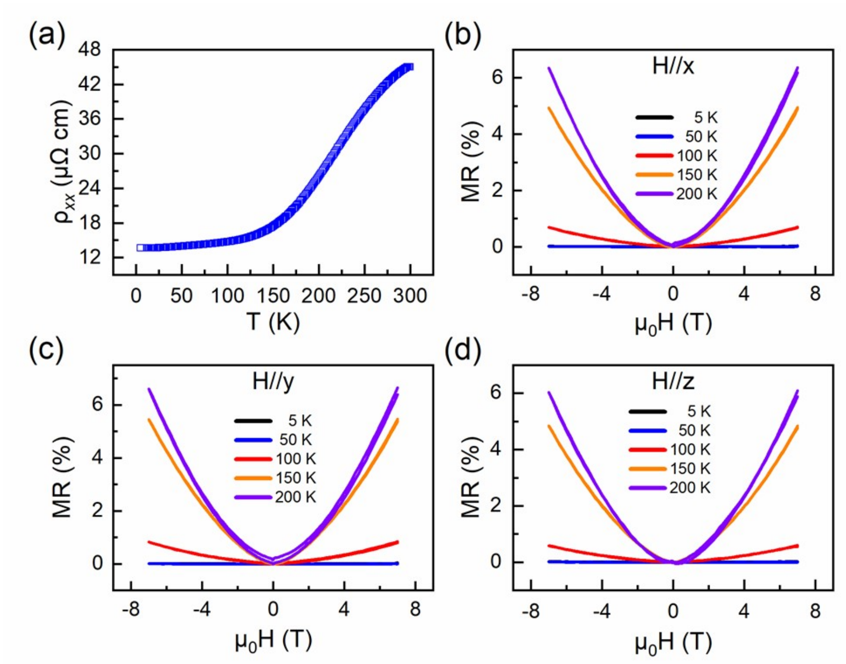

Fig. S10 (a) ρ_{xx}-T curve and (b)-(d) FDMR of Pt(3 nm)/LSMO(6 nm)/LAO [(b) $H // x$, (c) $H // y$, (d) $H // z$].

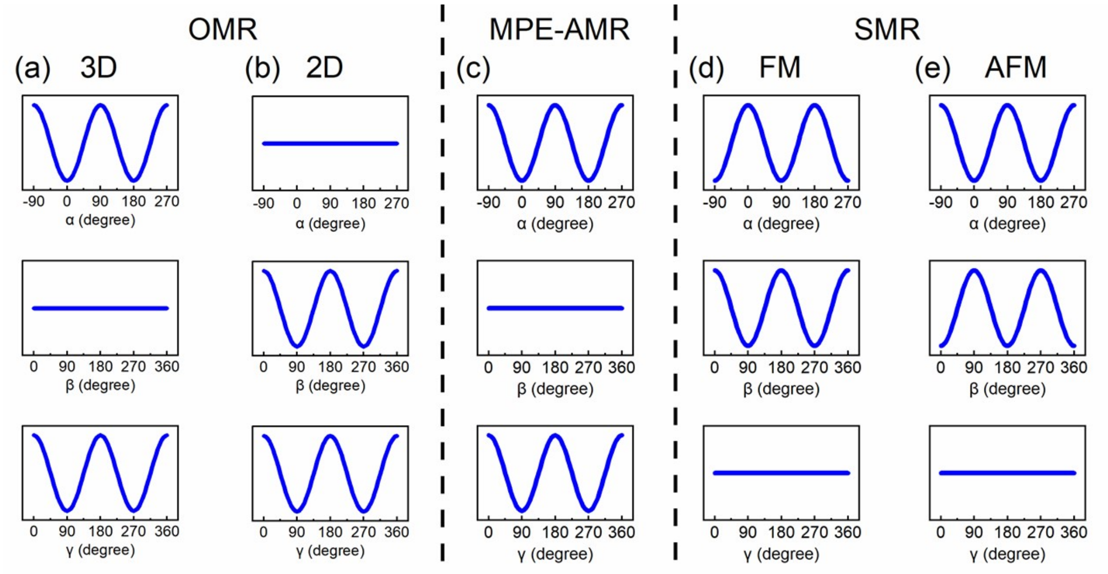

Fig. S11 Theoretical results of OMR, MPE-induced AMR, and SMR.

Theoretically, OMR exhibits a relatively low resistance for $H // I$ and a high resistance for $H \perp I$ in the three-dimensional (3D) system, i.e., there is an ADMR signal when H rotates in the *xy* and *xz* planes, but no signal in the *yz* plane, as shown in Fig. S11(a).[1] In the two-dimensional (2D) system, the movement of electrons is limited in the *xy* plane, and the Lorentz force causes the OMR in the *yz* and *xz* planes, showing the high resistance when $H // z$ [Fig. S11(b)].[2]

Due to the MPE, the Pt atoms near the magnet can produce magnetic moments and long-range ferromagnetic (FM) ordering,[3] further inducing the MPE-induced AMR, which can be observed in the *xy* and *xz* planes but does not exist in the *yz* plane, as shown in Fig. S11(c).[1]

In the heavy metal/FM insulator heterostructures, due to the SMR effect, a high (low) resistance state can be formed when the magnetization is perpendicular (parallel) to the spin accumulation at the interface.[4] Due to the spin accumulation along the *y*-axis, a change in the resistance can be observed when the magnetic field (magnetization) rotates in the *xy* and *yz* planes, as shown in Fig. S11(d). In the *xz* plane, the magnetization is always perpendicular to the spin accumulation, and the change in the resistance disappears. Therefore, the SMR can be observed in the *xy* and *yz* planes, but it disappears in the *xz* plane. In the heavy metal/AFM insulator heterostructures, the magnetization is no longer parallel to the magnetic field and forms a spin tilting towards the direction of the magnetic field.[5] Therefore, the SMR of the heavy metal/AFM insulator heterostructures has the opposite angular dependence in the *xy* and *yz* planes to the heavy metal/FM insulator heterostructures, as show in Fig. S11(e).[6]

Reference

(1) Amamou, W.; Pinchuk, I. V.; Trout, A. H.; Williams, R. E. A.; Antolin, N.; Goad, A.; O'Hara, D. J.; Ahmed, A. S.; Windl, W.; McComb, D. W.; Kawakami, R. K. Magnetic proximity effect in Pt/$CoFe_2O_4$ bilayers. *Phys. Rev. Mater.* **2018**, *2*, 011401.

(2) Baldrati, L.; Ross, A.; Niizeki, T.; Schneider, C.; Ramos, R.; Cramer, J.; Gomonay, O.; Filianina, M.; Savchenko, T.; Heinze, D.; Kleibert, A.; Saitoh, E.; Sinova, J.; Kläui, M. Full angular dependence of the spin Hall and ordinary magnetoresistance in epitaxial antiferromagnetic NiO(001)/Pt thin films. *Phys. Rev. B* **2018**, *98*, 024422.

(3) Nodo, S.; Ono, S.; Yanase, T., Shimada, T.; Nagahama, T.; Controlling the magnetic proximity effect and anomalous Hall effect in $CoFe_2O_4$/Pt by ionic gating. *Appl. Phys. Express.* **2020**, *13*, 063004.

(4) Nakayama, H.; Althammer, M.; Chen, Y.-T.; Uchida, K.; Kajiwara, Y.; Kikuchi, D.; Ohtani, T.; Geprägs, S.; Opel, M.; Takahashi, S.; Gross, R.; Bauer, G. E. W.; Goennenwein, S. T. B.; and Saitoh, E. Spin Hall Magnetoresistance Induced by a Nonequilibrium Proximity Effect. *Phys. Rev. Lett.* **2013**, *110*, 206601.

(5) Van Rijn, J. J. L.; Wang, D.; Sanyal, B.; and Banerjee, T. Strain-driven antiferromagnetic exchange interaction in $SrMnO_3$ probed by phase-shifted spin Hall magnetoresistance. *Phys. Rev. B* **2022**, *106*, 214415.

(6) Hoogeboom, G. R.; Aqeel, A.; Kuschel, T.; Palstra, T. T. M.; and van Wees, B. J.

Negative spin Hall magnetoresistance of Pt on the bulk easy-plane antiferromagnet NiO. *Appl. Phys. Lett.* **2017**, *111*, 052409.